int. J. Heat Mass Transfer. Vol. 33, No. 8, pp. 1721–1735, 1990
Printed in Great Britain

0017-9310/90 $3.00 + 0.00

Prediction of film condensation on horizontal integral fin tubes

THOMAS ADAMEK
Universität Stuttgart, D-7000 Stuttgart, F.R.G.

and

RALPH L. WEBB
Department of Mechanical Engineering, The Pennsylvania State University, University Park, PA 16802, U.S.A.

(*Received* 6 *March* 1989 *and in final form* 23 *October* 1989)

Abstract—This paper presents an analytical model for prediction of film condensation on horizontal integral fin tubes. The present model accounts for condensation on all surfaces in the flooded and unflooded regions, and includes the effect of fin efficiency. However, it is based on quite simple principles, and is applicable to hand or computer calculations. The model is applicable to fins of two different basic profile shapes: the special continuous profile shapes previously described by Gregorig, Adamek, or Webb, or fins having rectangular or trapezoidal cross-sections. The model is validated by showing its ability to predict a wide range of experimental data. The data include water, methanol, n-pentane, R-11, R-12, R-22 and R-113. These data for 80 different tube geometries are predicted within ±15%. Predictions by the present model are compared with models previously proposed by Webb *et al.*, Honda and Nozu, and Beatty and Katz.

1. INTRODUCTION

THIS PAPER presents a model for prediction of film condensation on horizontal integral fin tubes. The integral fin tubes usually have fins of a trapezoidal or possibly a rectangular cross-sectional shape. However, Webb *et al.* [1] and Rudy and Webb [2] have shown that surface tension drains the fins. This work showed that the fin profile need not have the special shapes described by Gregorig [3] or Adamek [4] for surface tension drainage to occur. Rudy and Webb [2] and Honda [5] showed that surface tension also acts to retain a thick layer of condensate on the lower side of the tube. Webb *et al.* [6] and Honda and Nozu [7] developed theoretical models to predict the condensation rate on such finned tubes. Webb *et al.* [6] assumed that the fin profile may be described by Adamek's profile equations [4], while the Honda and Nozu model assumed a rectangular fin cross-section. Webb *et al.* neglected the condensation rate in the condensate flooded region. Honda and Nozu used a numerical solution scheme, which included a methodology to predict the condensation rate on the fin sides and in the base channel for the unflooded and the flooded regions. Since the Honda and Nozu model requires numerical integration, it is not amenable to hand solution.

The present model may be considered to be competitive with the Honda and Nozu model in that it accounts for condensation on all surfaces in the flooded and unflooded regions. However, it is based on quite simple principles, and is applicable to hand or computer calculations. The model is applicable to fins of two different basic profile shapes: (1) the special continuous profile shapes as described by Gregorig [3], Adamek [4], or Webb [8], or (2) fins having rectangular or trapezoidal cross-sectional shapes.

The model is validated by showing its ability to predict a wide range of experimental data. The data include water, methanol, n-pentane, R-11, R-12, R-22 and R-113. Predictions by the present model are compared with the models of Webb *et al.* [6], Honda and Nozu [7], and Beatty and Katz [9]. Beatty and Katz were the first to propose a theoretical model for integral fin tubes. This assumed that the condensate was gravity drained, and that no condensate retention existed.

2. DEFINITION OF CONDENSATION ZONES

Figure 1 shows an end cross-section view of the finned tube. The diameter over the fins is D_0 and the diameter at the base of the fins is D_r. The interfin region in the shaded portion of the lower tube circumference is totally condensate flooded. The flooding half angle Ψ_0 is given by equation (1), which was independently derived by Rudy and Webb [3, 10] and Honda [5]

$$\Psi_0 = \cos^{-1}[1 - 4\sigma/(D_0 s \rho g)]. \quad (1)$$

The condensation is divided into three distinct zones.

(1) The unflooded zone: this is the fraction of the

NOMENCLATURE

A	area of cross-section of drainage with circular shape [m^2]
A_b	cross-sectional area (for heat conduction) at base of fin [m^2]
A_f	surface area of fin side [m^2]
A_r	surface area of tube at fin root [m^2]
A_t	surface area of fin tip [m^2]
A_{tub}	total surface area of tube, $A_f+A_r+A_t$ [m^2]
d_H	hydraulic diameter, $4A/P$ [m]
D_r	tube diameter to the fin root [m]
D_0	tube diameter to outside of the fin [m]
f	friction factor for drainage at fin root
f_{ik}	force per unit volume within region L_{ik} [N m^{-3}]
F_p	property group $4kv\Delta T/\lambda$ [N]
g	gravitational constant [m s^{-2}]
h	condensing coefficient, h_f on fins, h_{fl} in flooded region, h_r at fin root [W m^{-2} K^{-1}]
h_t	condensation coefficient at the fin tip [W m^{-2} K^{-1}]
h	height of fin [m]
h_{tub}	heat transfer coefficient based on A_{tub} [W m^{-2} K^{-1}]
k	thermal conductivity of condensate [W m^{-1} K^{-1}]
k_w	thermal conductivity of the fin [W m^{-1} K^{-1}]
l_{ik}	length between points $x=i$ and k [m]
L_{ik}	region between points $x=i$ and k
L	tube length [m]
$\dot{m}_{ik}$	condensate (flow) rate on region L_{ik} [kg s^{-1} m^{-1}]
$\dot{m}_t$	condensate generated on fin tip [kg s^{-1} m^{-1}]
$\dot{m}_{t,\infty}$	condensate generated on fin tip for infinite fin conductivity [kg s^{-1} m^{-1}]
$\dot{M}$	drainage flow rate in z-direction [kg s^{-1}]
$\dot{M}_{fl}$	condensation rate in flooded region of tube [kg s^{-1}]
$\dot{M}_u$	condensation rate in unflooded region of tube [kg s^{-1}]
$\dot{M}_{ik}$	total condensate rate between points $x=i$ and k [kg s^{-1}]
$\dot{M}_{tub}$	total condensation rate on tube, M_u+M_{fl} [kg s^{-1}]
N	fins/m on tube [m^{-1}]
Nu_t	fin tip Nusselt number, $h_t h/k_w$
P	wetted perimeter [m]
Δp	pressure difference compared to saturation pressure [N m^{-2}]
Q	total condensation rate on tube, Q_{pred} (predicted), Q_{exp} (experimental) [W]
q	heat flow in fin (equations in Appendix A) [W]
r	local radius of condensate interface [m]
R^*	$R-\delta_{54}$, projection of R on side wall from point 4 of Fig. 3(c) [m]
R	radius of drainage interface at fin root [m]
s	space between two adjacent fins, fin spacing [m]
T_{sat}	vapor saturation temperature [K]
T_w	surface temperature, $T_{w,r}$ (at fin root), $T_{w,t}$ (at fin tip) [K]
ΔT	temperature difference, T_w-T_{sat} [K]
t	fin thickness at the tip [m]
x	direction on fin surface from tip to base [m]
w	condensate film velocity [kg s^{-1}]
z	direction of drainage flow at tube [m].

Greek symbols

α	angle in Fig. 3(c) [rad]
β	angle in Fig. 3(c) [rad]
δ_{ik}	film thickness in section L_{ik} [m]
Δ	condensate film thickness in the channel [m]
η	dynamic viscosity of condensate [kg s^{-1} m^{-1}]
η_f	fin efficiency
θ	temperature difference, T_w-T_{sat} [K]
θ	angle at fin tip in Fig. 2 [rad]
$\theta'(x)$	derivative of θ with respect to x [K m^{-1}]
θ_t	temperature difference, $T_{w,t}-T_{sat}$ [K]
$\theta_{t,\infty}$	temperature difference, $T_{w,r}-T_{sat}$ [K]
κ	curvature of interface [m^{-1}]
$\kappa'(s)$	derivative of κ with respect to s [m^{-2}]
λ	latent heat of vaporization of condensate [W s kg^{-1}]
v	kinematic viscosity of condensate [m^2 s^{-1}]
ρ	density of condensate [kg m^{-3}]
σ	surface tension of condensate [N m^{-1}]
τ_w	wall shear stress [N m^{-2}]
Ψ	angle in Fig. 1 [rad]
Ψ_0	condensate retention angle in Fig. 1 [rad]
$\omega, \omega', \omega''$	angle on fin tip (Fig. 3) [rad].

Subscripts

bot	bottom
drai	drainage
fin	fin
fl	flooded area
sid	side
tip	tip
tub	tube
u	unflooded area.

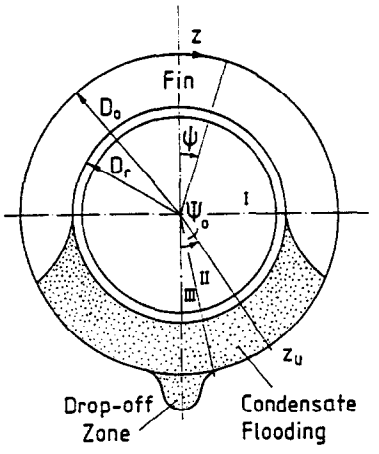

FIG. 1. Illustration of condensate retention and definition of condensation zones. I, Unflooded zone (u); II, flooded zone (fl); III, drop-off zone.

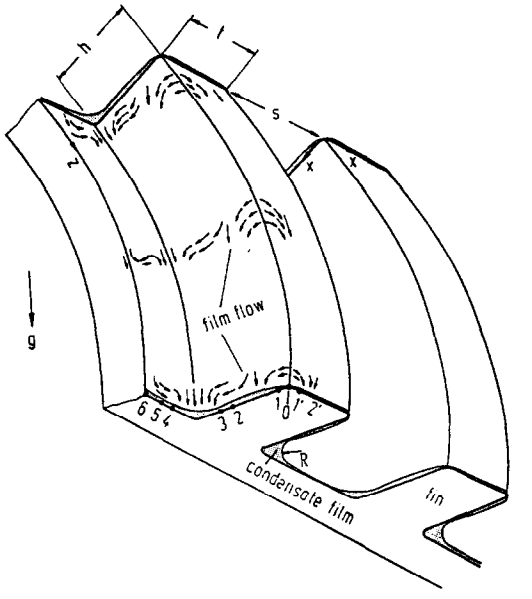

FIG. 2. Illustration of condensate flow pattern assumed by the model.

tube circumference outside the shaded region of Fig. 1. It consists of the fin tips and sides, and the base tube between the fins.

(2) The flooded zone: the model assumes that condensation occurs only on the fin tips in the flooded zone. Negligible condensation will occur on the liquid surface in the interfin region, because the interfin region is totally flooded.

(3) The drop-off zone: as shown by Fig. 1, gravity forms a heavy pendant of condensate, which insulates the fin tips. Based on experimental observations, this is taken to be 10% of the tube circumference.

It is necessary to develop theoretical equations for condensation in the flooded and unflooded zones.

3. CONDENSATION IN THE UNFLOODED ZONE

3.1. *Structure of the model*

Figure 2 is a sketch of the finned tube in the unflooded zone. It defines the geometric dimensions, the coordinate system, and the condensate flow regions to be modeled. Figure 3(a) shows a detailed view of these flow regions. The film surface in Fig. 3(a) is divided into segments L_{ik}. The indices ik define the initial point $x = i$ and the end point $x = k$ of the region L_{ik}. The lengths of these sections are denoted by the terms l_{ik}. The expressions $\dot{m}_{ik}$ define the condensation rates between points $x = i$ and k per unit of the tube circumference (the z-direction). The total condensation rate on one half of the fin per unit length in the circumferential direction is

$$\dot{m}_u = \dot{m}_{1'2'} + \dot{m}_{01'} + \dot{m}_{01} + \dot{m}_{12} + \dot{m}_{23} + \dot{m}_{54} + \dot{m}_{65}. \tag{2a}$$

The total condensation rate, $\dot{m}_u$, is made up of the partial contributions at the fin tip $\dot{m}_{tip}$, at the lateral fin side $\dot{m}_{sid}$ and at the bottom $\dot{m}_{bot}$. Thus

$$\dot{m}_u = \dot{m}_{tip} + \dot{m}_{sid} + \dot{m}_{bot} = \dot{m}_{fin} + \dot{m}_{bot} \tag{2b}$$

where

$$\begin{aligned} \dot{m}_{tip} &= \dot{m}_{02'} = \dot{m}_{01'} + \dot{m}_{1'2'} \\ \dot{m}_{sid} &= \dot{m}_{03} = \dot{m}_{01} + \dot{m}_{12} + \dot{m}_{23} \\ \dot{m}_{bot} &= \dot{m}_{65} + \dot{m}_{54} = \dot{m}_{64} \\ \dot{m}_{fin} &= \dot{m}_{tip} + \dot{m}_{sid} = \dot{m}_{2'3}. \end{aligned} \tag{3}$$

For the analysis of the radius R of interface at the fin base, we need the expression $\dot{m}_{drai}$, denoting the sum of all condensation rates, which flow to the fin base (Fig. 2)

$$\dot{m}_{drai} = \dot{m}_{sid} + \dot{m}_{54}. \tag{4}$$

All expressions for $\dot{m}_{ik}$ vary in the circumferential z-direction. Figure 2 shows that the condensate $\dot{m}_{tip}$ and $\dot{m}_{65}$ do not flow to the fin base. Rather, their drainage direction is determined by gravity force. The integration of the differential condensation rates $\dot{m}_{ik}(z)$ from the top of the tube ($z = 0$) to the circumferential length z is indicated by the terms $\dot{M}_{ik}(z)$. Thus

$$\dot{M}_{ik}(z) = \int_0^z \dot{m}_{ik}(t)\,\mathrm{d}t. \tag{5}$$

If $z_u = (\pi - \Psi_0)D_0/2$ denotes the unflooded circumference of the tube in Fig. 1, the total condensation rate per one half of the fin is defined by

$$\begin{aligned} \dot{M}_u(z_u) &= \dot{M}_{tip}(z_u) + \dot{M}_{sid}(z_u) + \dot{M}_{bot}(z_u) \\ &= \int_0^{z_u} \dot{m}_{tip}(z) + \dot{m}_{sid}(z) + \dot{m}_{bot}(z)\,\mathrm{d}z. \end{aligned} \tag{6}$$

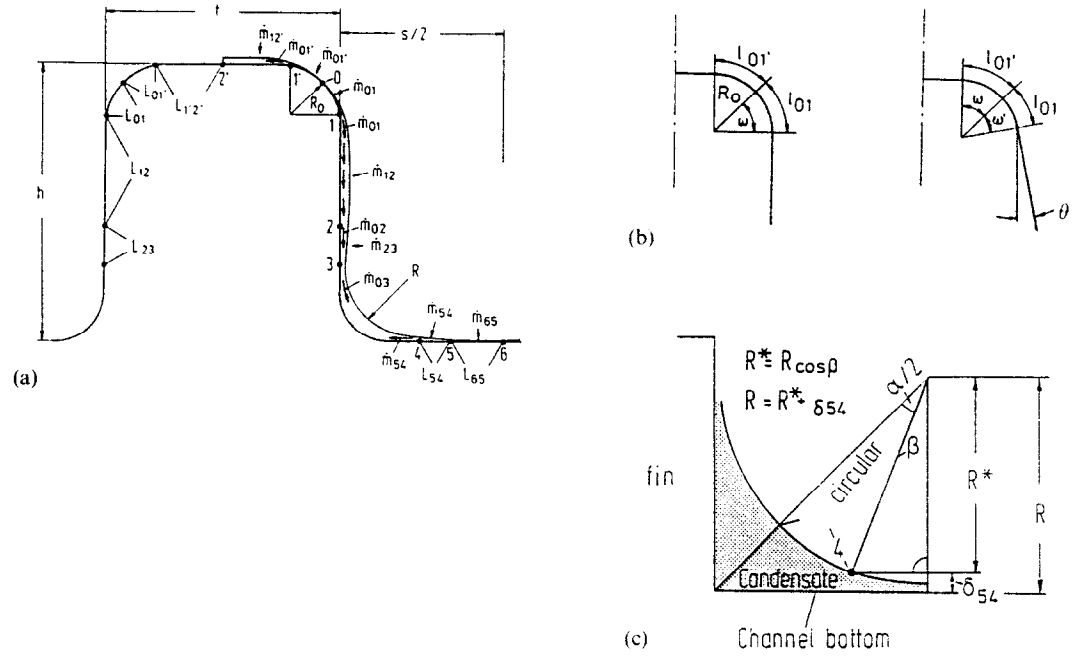

FIG. 3. (a) Cross-section of fin and root illustrating the defined condensate drainage regions (not to scale). (b) Detail of fin tip corner: left, rectangular fin; right, trapezoidal fin. (c) Detail of drainage in corner of drainage channel.

The condensation rate in the unflooded portion of the tube is given by

$$\dot{M}_{\text{tub.u}} = 4N\dot{M}_{\text{u}} \tag{7}$$

where N defines the number of fins on the tube length.

The condensate films are drained either by gravity or surface tension forces. The key hypothesis of the model is to identify the forces, which are active for each region L_{ik}. Once the dominant force is identified, one may calculate the film thickness associated with the particular L_{ik} region. For laminar film condensation, the local condensation coefficient is $h = k/\delta$, where k is the thermal conductivity of the condensate, and δ is the local film thickness. Hence, if the local film thickness can be calculated, the local condensation coefficient is easily determined.

3.2. *Basic equations for calculation of film thickness*

For gravity drained laminar film condensation on an inclined plate of length l, Nusselt [11] showed that the local film thickness at $x = l$ is given by

$$\delta(l) = [F_{\text{p}} \cdot l/\rho g \cdot \cos \Psi]^{1/4} \tag{8}$$

where $F_{\text{p}} \equiv 4k\nu\Delta T/\lambda$. The condensate generated on a plate of length l is

$$\dot{m}(l) = 0.943[(k\Delta T \cdot l/\lambda)^3(\rho g/\nu) \cdot \cos \Psi]^{1/4} \tag{9}$$

where Ψ is the angle of the plate relative to the vertical direction.

Now consider calculation of the film thickness, if surface tension is the dominant drainage force in region L_{ik}. The surface tension induced pressure gradient is

$$\mathrm{d}p/\mathrm{d}s = -\sigma \mathrm{d}(1/r)/\mathrm{d}s \tag{10a}$$

where r is the local radius of the condensate interface. We will assume that a linear pressure gradient exists in all such surface tension drained regions. Hence, for a generalized region L_{ik}

$$\mathrm{d}p/\mathrm{d}s \equiv f_{ik} = -\sigma[(1/r_k) - (1/r_i)]/l_{ik} \tag{10b}$$

where r_i and r_k are the radii at the beginning and end of the length l_{ik}, respectively, and f_{ik} symbolizes the pressure gradient for region L_{ik}. This simple modeling concept was initially proposed by Rifert [12] and was used by Rudy [13] to model the surface tension drainage gradient on integral fin tubes.

One may modify equations (8) and (9) to apply to a surface tension drained plate of length l_{ik}. The gravity force per unit volume in equation (8) ($\rho g \cdot \cos \Psi$) may be replaced by f_{ik}, equation (10b). The length over which equation (10b) applies, l_{ik}, corresponds to l in equation (8). The result is

$$\delta_{ik}(l_{ik}) = [F_{\text{p}}(l_{ik}/f_{ik})]^{1/4} \tag{11}$$

$$\dot{m}(l_{ik}) = 0.943[(k\Delta T/\lambda)^3 f_{ik} l_{ik}^3/\nu]^{1/4},$$

$$ik = 01', 01 \text{ and } 54$$

$$\dot{m}(l_{ik}) = \frac{\Delta T}{\lambda}\int_0^{l_{ik}} \frac{k}{\delta_{ik}(x)}\,\mathrm{d}x, \quad ik = 12 \text{ and } 23. \tag{12a,b}$$

Equations (11) and (12) may be used to calculate the film thickness and condensation rate in each of the surface tension drained regions L_{ik} of Fig. 3(a), if f_{ik} and l_{ik} can be defined for each region.

3.3. *Specification of forces governing film flow in regions* L_{ik}

Figures 2 and 3 will be used to establish the drainage forces acting in regions L_{ik}. The fin shape is shown as rectangular, but the model may be equally applied also to trapezoidal fins. The corner of the fin tip is assumed to be circular with radius R_0, as shown in Fig. 3(a). Hence the interface changes within the sections L_{01} and $L_{01'}$ from a circular to a linear shape, which is associated with a pressure drop of $\Delta p_{01'} = \Delta p_{01} = \sigma/R_0$ (Fig. 4). Neglecting gravity in these sections, the film flow is governed by surface tension force and follows the x-direction.

In region $L_{1'2'}$ the interface is linear and the surface tension forces are small compared to gravity. Hence the condensation process is gravity dominated, and the film flows approximately in the circumferential direction.

Gravity also dominates in section L_{12}. If we define a circumferential angle $\Psi = 2z/D_0$ (Fig. 1), then we may express the forces in the x-direction and the z-direction by the terms $\rho g \cos \Psi$ and $\rho g \sin \Psi$, respectively. Thus, the direction of the film flow is defined by the vector $(\cos \Psi, \sin \Psi)$.

Between points 2 and 3, the interface changes from a linear to a circular shape, which is associated with a pressure drop of magnitude $\Delta p_{23} = \sigma/R$ (Fig. 4). Hence, the condensation process in L_{23} is governed by surface tension, and the film flow is assumed to occur in the x-direction.

The area L_{34} at the fin base is assumed to be the drainage center. Although the interface changes to a concave shape, the radius R of curvature remains constant. So, the pressure drop between points 3 and 4 remains zero, and the drainage flow occurs only in the circumferential z-direction.

In contrast, between points 4 and 5 the interface changes from a circular to a linear shape, which is associated with a pressure drop $\Delta p_{54} = \sigma/R$. Note that the pressure at point 5 is higher than at point 4, which causes the film to flow into the corner.

Finally, the interface in the region L_{65} remains linear, so the flow is gravity dominated, and the film flows in the circumferential z-direction.

Note that the condensate from regions L_{01}, L_{12}, L_{23} and L_{54} accumulates in the corner at the fin base. Accordingly, the interface radius in the corner, R, increases in the z-direction. So, the lengths l_{ik} in regions L_{ik} vary with respect to the variable z.

3.4. *Calculation of condensation rates* $\dot{m}_{01}$ *and* $\dot{m}_{01'}$

As shown in Fig. 3(b), the corner of the fin tip is assumed to be circular with radius R_0. In the real case, the shape may not be exactly circular, but a small radius R_0 will exist at the curved fin edge. We will assume a linear pressure decrease $\Delta p_{01} = \sigma/R_0$ and $\Delta p_{01'} = \sigma/R_0$ from the center of radius to the lateral fin wall and to the fin tip, respectively. This results in the linear curvature gradient shown in Fig. 4 for regions L_{01} and $L_{01'}$. The film radius becomes infinite (zero curvature) at the inflection points, 1 and 1'. Using equation (10b), we obtain for the pressure gradients

$$f_{01} = \sigma/R_0 l_{01}, \quad f_{01'} = \sigma/R_0 l_{01'}. \qquad (13a,b)$$

The angle ω is equal to the change of curvature over $l_{01'}$. As shown by Fig. 4, this curvature change is the area under the triangle bounded by $1/R_0$ and $l_{01'}$. Thus, lengths l_{01} and $l_{01'}$ are calculated by

$$l_{01} = 2R_0\omega', \quad l_{01'} = 2R_0\omega. \qquad (14a,b)$$

The case of rectangular and trapezoidal fin shapes are shown in Fig. 3(b). For rectangular fins, $\omega = \omega' = \pi/4$, and for trapezoidal fins, $\omega = \pi/4$, and $\omega' = \pi/4 - \omega''$. Substitution of equations (13a) and (14a) in equations (11) and (12) gives

$$\delta_{01}(x) = 1.189[F_p(R_0^2\omega' x/\sigma)]^{1/4},$$
$$\delta_{01'}(x) = 1.189[F_p(R_0^2\omega x/\sigma)]^{1/4}. \qquad (15a,b)$$

Application of equation (12) gives

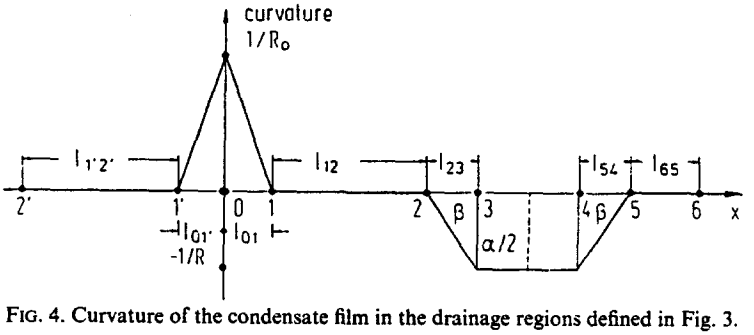

FIG. 4. Curvature of the condensate film in the drainage regions defined in Fig. 3.

$$\dot{m}_{01} = 1.332[(k\Delta T/\lambda)^3(\sigma R_0\omega'^2/\nu)]^{1/4},$$

$$\dot{m}_{01'} = 1.332[(k\Delta T/\lambda)^3(\sigma R_0\omega^2/\nu)]^{1/4}. \quad (16a,b)$$

3.5. *Calculation of radius R at the fin root*

The determination of the condensation terms $\dot{m}_{12}$, $\dot{m}_{23}$, $\dot{m}_{54}$ and $\dot{m}_{65}$ depend on the condensate radius R at the fin root. Gravity drains the condensate at the fin root in the circumferential z-direction. This mass flow rate is defined by the continuity equation

$$\dot{M}(z) = \rho \cdot w(z) \cdot A(z) \quad (17)$$

where the average film flow velocity $w(z)$ in the circumferential z-direction is governed by

$$\tau_w = f(\rho w^2/2) = (A/P)\rho g \cdot \sin\Psi \quad (18)$$

and

$$f = 12/Re = 12\nu/(d_H w) \quad (19)$$

where τ_w is the wall shear stress on the surface area $P \cdot dz$ balanced by the film weight $[A \cdot dz \cdot \rho g \cdot \sin\Psi]$, with wetted perimeter $P = 2R$ and cross-section $A = 0.215R^2$ for rectangular fins. The expressions for A and P are calculated from the geometry of the circular interface at the fin base. The number 12 in equation (19) is taken from Thomas [14]. From equations (17)–(19) we obtain

$$w = (g d_H^2 \cdot \sin\Psi)/24\nu \quad (20)$$

and

$$\dot{M}(z) = 0.0017[\rho g \cdot \sin\Psi \cdot R^4(z)/\nu] \quad (21)$$

where $d_H = 4A/P = 0.43R$.

Note that the drainage mass flow is related to the fourth power of $R(z)$, so imprecision in the calculation of $\dot{M}(z)$ will yield a very small error in $R(z)$. If the fin has a radius at the root, the shape at the base is circular rather than rectangular, so we may replace the number 12 in equation (19) by the number 14.25, as specified by Honda *et al.* [15]. A finite element analysis for the determination of the drainage mass flow was performed to verify both numbers. For the rectangular and circular cases, we obtained the numbers 13.2 and 15.3, respectively. The radius R is obtained by equating equation (21) with the sum of the condensation rates that flow into the fin root region, $\dot{M}_{drai}$.

From equations (4) and (21) we obtain

$$R(z) = \left(\frac{\nu}{0.0017\rho g \sin\left(\dfrac{2z}{D_r}\right)} \int_0^z \dot{m}_{sid}(t) + \dot{m}_{54}(t)\, dt \right)^{1/4} \quad (22)$$

where $\dot{m}_{sid} = \dot{m}_{01} + \dot{m}_{12} + \dot{m}_{23}$.

Unfortunately, the expressions $\dot{m}_{12}$, $\dot{m}_{23}$ and $\dot{m}_{54}$ depend on R, which leads to a complicated iterative solution. However, a good approximation is possible by noting that $\dot{m}_{01}$ is the main contributor to $\dot{m}_{drai}$, and that $R(z)$ is not very sensitive to $\dot{M}_{drai}$. This procedure involves the following steps.

(1) Estimate $\dot{m}_{drai} = 1.3\dot{m}_{01}$.

(2) Calculate $R(z)$ by equation (22) with the integrand replaced by $1.3\dot{m}_{01}(t)$.

(3) Analyze the lengths $l_{12}(z)$, $l_{23}(z)$, $l_{54}(z)$, $l_{65}(z)$, $l_{1'2'}(z)$ and the corresponding condensation rates $\dot{m}_{ik}(z)$ using $R(z)$ obtained from the modified equation (22). This allows calculation of $\dot{m}_{sid}$ and $\dot{m}_{54}$.

(4) Using the known $\dot{m}_{sid}$ and $\dot{m}_{54}$, use equation (22) as given to recalculate $R(z)$.

The analysis for step 3 above is described in the next section.

3.6. *Condensation rate on the fin and base*

Calculation of the condensation rate on the sides and at the fin base requires specification of l_{12}, l_{23}, l_{54}, l_{65} and R illustrated in Fig. 3(a). The model assumes that l_{23} and l_{54} are surface tension drained, and that l_{12}, l_{34} and l_{65} are gravity drained. The basis of these assumptions is illustrated in Fig. 4. The l_{ij} which have constant curvature are gravity drained. With these l_{ij} and R known, we may use equations (12) and (16) to calculate the associated $\dot{m}_{ij}$. The l_{ij} terms may be related to the fin dimensions t, h, θ and the fin spacing s as shown below

$$t/2 = R_0 + l_{1'2'} \quad (23)$$

$$h = \cos\theta(R_0 + l_{12} + l_{23} + R^* + \Delta) \quad (24)$$

where Δ is the condensate thickness at the fin root. At the fin root

$$s/2 = h\sin\theta + R^* + l_{54} + l_{65} \quad (25)$$

where $R^* \equiv R - \delta_{54} = R\cos\beta$, as shown by Fig. 3(c). Using the linear pressure gradient assumption, the area of the $\kappa - l_{54}$ triangle in Fig. 4 yields the relation $\beta = (l_{54}/2)(1/R)$, where β is the area under the triangle. Thus

$$R^* = R\cos(l_{54}/2R). \quad (26)$$

The Appendix of Adamek and Webb [16] shows that

$$l_{23} = l_{54} = 4[F_p R^5/\sigma]^{1/6}. \quad (27)$$

Using the known R_0 and l_{23}, l_{54} and R^* from equations (26) and (27), one may solve equations (23)–(26) for $l_{1'2'}$, l_{12} and l_{65}.

With the l_{ik} known, one may directly write the forces f_{ik} acting on each L_{ik} region. Linear surface tension pressure gradients acting on L_{01}, $L_{01'}$, L_{23} and L_{54} yield

$$f_{01'} = \sigma/R_0 l_{01} \quad (13a)$$

$$f_{01} = \sigma/R_0 l_{01} \quad (13b)$$

$$f_{23} = \sigma/R l_{23} \quad (28)$$

$$f_{54} = \sigma / Rl_{54}. \quad (29)$$

Region L_{12} is gravity drained. The gravity force components in the x- and z-directions ($\rho g \cdot \cos \Psi$ and $\rho g \cdot \sin \Psi$, respectively) change with the circumferential angle Ψ. A rigorous analysis would require solving for the film thickness in the streamline direction, resulting from the two force components. However, previous analysis by Adamek [17] has shown that this complication is not warranted. For a condensation process governed by two perpendicular forces, the analysis showed that the calculated film thickness in one coordinate direction is nearly independent of the other force. The present model will calculate the x-component of the average gravity force, which gives

$$f_{12} = \frac{2}{\pi}\int_0^{\pi/2} \rho g \cos \psi \, d\psi = \frac{2}{\pi}\rho g. \quad (30)$$

The gravity force in regions $L_{1'2'}$ and L_{65} act on the fin tip and on the base tube, respectively. The single gravity component is $\rho g \cdot \sin \Psi$, which results in

$$f_{1'2'} = \rho g \cdot \sin \Psi \quad (31)$$

$$f_{65} = \rho g \cdot \sin \Psi. \quad (32)$$

The film thickness equations for the surface tension drained regions is obtained by substituting the l_{ik} and f_{ik} terms in equation (11), giving

$$\delta_{01}(x) = (2F_p R_0^2 \omega' x/\sigma)^{1/4} \quad (15a)$$

$$\delta_{01'}(x) = (2F_p R_0^2 \omega x/\sigma)^{1/4} \quad (15b)$$

$$\delta_{23}(x) = [(3\nu \dot{m}_{02} Rl_{23}/\sigma)^{4/3} + F_p Rl_{23} x/\sigma]^{1/4} \quad (33)$$

$$\delta_{54}(x) = (F_p Rl_{54} x/\sigma)^{1/4}. \quad (34)$$

Equation (33) includes two terms on the right-hand side. The first term accounts for the fact that L_{23} receives flow from region L_{12}. The supporting derivation of equation (33) is provided in Appendix 1 of Adamek and Webb [16].

The film thickness for the gravity drained regions is obtained by substituting the l_{ik} and f_{ik} terms in equation (8) giving

$$\delta_{1'2'} = \delta_{1'2'}(z) = \left(\left(\frac{F_p}{\rho}\right) \frac{\int_0^z \left(g \sin\left(\frac{2z}{D_0}\right) dz \right)^{1/3}}{\left(g \sin\left(\frac{2z}{D_0}\right)\right)^{4/3}} \right)^{1/4} \quad (35)$$

$$\delta_{12} = \{(3\nu\pi \dot{m}_{01}/2\rho g)^{4/3} + [F_p(\pi/2\rho g)x]\}^{1/4} \quad (36)$$

$$\delta_{65} = \delta_{65}(z) = \left(\frac{F_p}{\rho} \frac{\int_0^z \left(g \sin\left(\frac{2z}{D_r}\right) dz \right)^{1/3}}{\left(g \sin\left(\frac{2z}{D_r}\right)\right)^{4/3}} \right)^{1/4}. \quad (37)$$

Equation (36) also contains two terms on the right-hand side. This is because L_{12} receives condensate from L_{01}.

With equations for δ_{ik} specified, the condensate generated in each L_{ik} may be calculated. Equation (12a) is used for surface tension drained regions $L_{01'}$, L_{01} and L_{54}. Regions L_{12} and L_{23} receive condensate flow from upstream. Hence, their condensation rates are calculated using equation (12b), with $\delta_{ik}(x)$ given by equations (33) and (36). Regions $L_{1'2'}$ and L_{65} are gravity drained in the z-direction. Their condensation rates are given by equation (5) with $\dot{m}_{ik}(t) = l_{ik}(t) \cdot \Delta T/\lambda \cdot k/\delta_{ik}(t)$ and δ_{ik} from equations (35) and (37).

The concave radius R varies in the circumferential direction (z). Hence, $\dot{m}_{1'2'}$, $\dot{m}_{12}$, $\dot{m}_{23}$, $\dot{m}_{54}$ and $\dot{m}_{65}$ will vary in the z-direction. Evaluation of these terms will require incremental calculations.

3.7. *Integration over z in the unflooded region*

The total z-length over which the solution is required is

$$z_u = D_0(\pi - \Psi_0)/2. \quad (38)$$

We will perform the integration by solving the $\dot{m}_{ik}$ equations over P-increments in the z-direction and calculating the total condensation rate $\dot{M}_j$ in each increment. The total condensation rate in the unflooded regions is the sum of the P_j values for each increment. The integration will start at the top of the tube ($z = 0$), and the values of R and δ_{ik} will be assumed constant within the increment. Assuming that the $\dot{m}_{sid} + \dot{m}_{54} = 1.3\dot{m}_{01}$, equation (22) simplifies to equation (39) for the initial estimate of R for the first z-increment

$$R^{(1)} = \lim \left(\frac{\nu}{0.0017 \rho g \sin\left(\frac{2z}{D_r}\right)} \int_0^z 1.3\dot{m}_{01} \, dt \right)^{1/4} = \left(\frac{\nu 1.3 \dot{m}_{01} D_r}{0.0017 \rho g 2} \right)^{1/4}. \quad (39)$$

Equation (39) includes the approximation

$$\lim_{y \to 0} \frac{y}{\sin y} = 1. \quad (40)$$

With the estimated R for the first increment known, equations (23)–(27) are solved for R^* and the required l_{ik}. The corresponding f_{ik} and δ_{ik} are then obtained from equations (13a), (13b), (15a), (15b), and (28)–(37). Application of the previously specified equations for l_{ik} yields the $\dot{m}_{ik}$ values. Finally, summation of the $\dot{m}_{ik}$ provides $\dot{M}_u$ for the first z-increment. For greater precision, one may repeat the calculation for the first increment using equation (22) to calculate R.

The starting value of R for the second z-increment is calculated using the converged $\dot{m}_{sid}+\dot{m}_{54}$ in equation (22). This procedure is repeated for all succeeding z-increments. Finally, the total condensation rate in the unflooded region ($\dot{M}_u$), per one half fin is the summation of the incremental $\dot{M}_u$ values. The condensation rate on the unflooded portion of the total tube length is

$$\dot{M}_{tub,u} = 4NL\dot{M}_u \quad (41)$$

where N is the fins/m and L is the tube length.

3.8. *Inclusion of fin efficiency*

The above analysis has assumed that ΔT = constant on all of the L_{ik}. The accuracy will be improved by accounting for the change of fin temperature along the fin length, thus accounting for fin efficiency, η_f. This development is presented in Appendix A. Then, the condensation rate on the fin is expressed by

$$\dot{M}_{fin} = \eta_f(\dot{M}_{12'}+\dot{M}_{01'}+\dot{M}_{01}+\dot{M}_{12}+\dot{M}_{23}). \quad (42)$$

The model assumes that condensation regions L_{23} and L_{12} both exist on the fin sides. However, if the tube diameter is large, or the condensation rate is high, it is possible that either of these two regions may not exist on some portion of the tube circumference. Thus, as the tube circumference is progressed, R, δ_{54} and δ_{65} will increase. The first region to disappear is L_{23}, followed by L_{12}. Appendix B provides criteria for determination of which regions will exist. These criteria may be included in the computer program.

It is probable that ΔT in the flooded and unflooded regions are different. It is possible to account for this difference. However, one must expand the concept of the model to account for circumferential conduction in the tube wall. This also requires specification of a tube side heat transfer coefficient. Honda and Nozu [7] outlined the methodology for doing this.

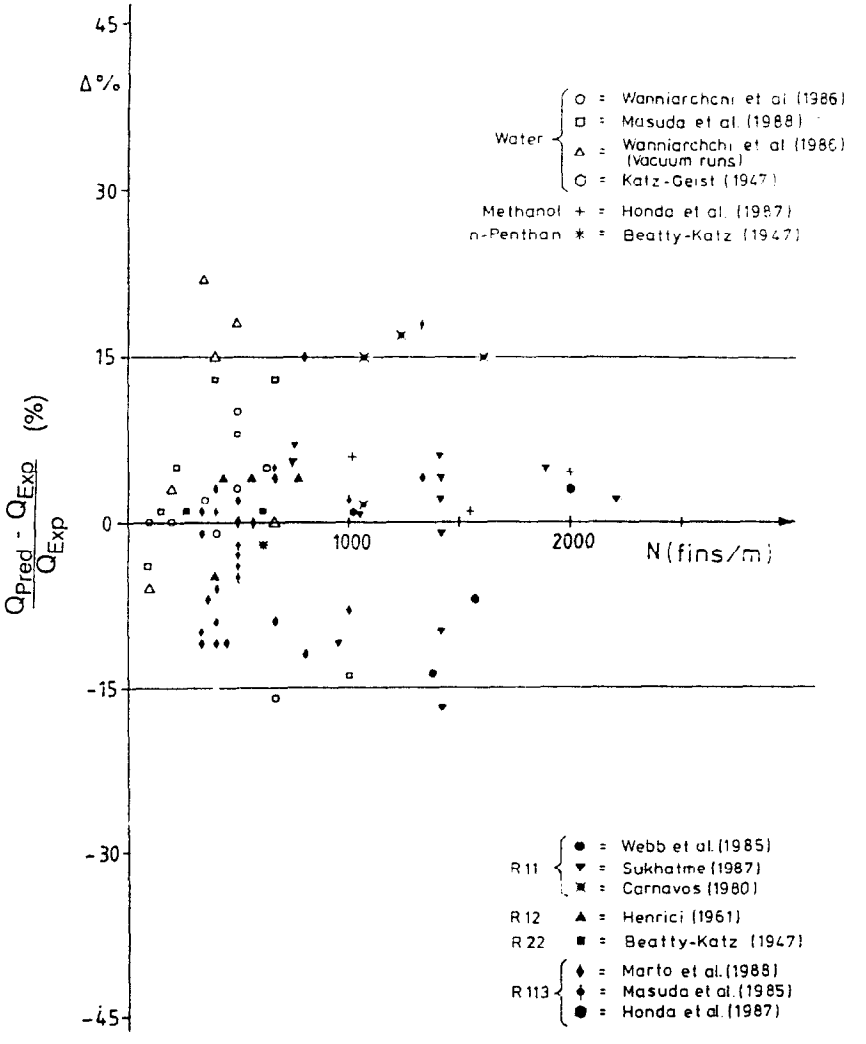

FIG. 5. Evaluation of the ability of the proposed model to predict the condensation rate on 80 tube geometries for seven fluids, $(Q_{pred}-Q_{exp})/Q_{exp}$ vs fins/m.

4. CONDENSATION IN THE FLOODED REGION AND THE TOTAL CONDENSATION RATE

As shown by Fig. 2, the interfin region is totally flooded with condensate for $\Psi \geqslant \Psi_0$. However, condensation will occur on the fin tips. Further, it is assumed that the previously described drop-off zone accounts for 10% of the tube circumference. The fin tips are covered with a heavy condensate thickness, so no condensation will occur on the fin tips. The fraction of the flooded region outside of the drop-off zone is called the 'active' flooded region. The condensation rate in the active flooded region, per one half fin, is given by

$$\dot{M}_{fl} = (D_0/2)(\Psi_0 - 0.1\pi)(\dot{m}_{1'2'} + \dot{m}_{01'}). \quad (43)$$

Having computed the total condensation rate in the unflooded region, $\dot{M}_u$, and the flooded region, $\dot{M}_{fl}$, the total condensation rate on the tube is

$$\dot{M}_{tub} = 4NL(\dot{M}_u + \dot{M}_{fl}). \quad (44)$$

The heat transfer rate is $Q = \dot{M}_{tub}/\lambda$. The heat transfer coefficient may be derived from the predicted value of $\dot{M}_{tub}$. This is done as follows:

$$h_{tub} = Q/(A_{tub}\lambda\Delta T) \quad (45)$$

where A_{tub} is the total surface area and is composed of

$$A_{tub} = NL(A_f + A_r + A_t) \quad (46)$$

and A_f, A_r and A_t are the surface areas of the fin side, root and tip, respectively.

Equation (45) assumes $\eta_f = 1.0$. If the fin efficiency is not one, one should calculate the heat transfer coefficients associated with the fin (h_f), root (h_r) and flooded (h_{fl}) regions. The surface efficiency is then defined as

$$\eta = [(\eta_f h_f A_f + h_r A_r)(\pi - \Psi_0) + h_{fl} A_t(\Psi_0 - 0.1\pi)]/(A_f + A_r). \quad (47)$$

Equation (47) assumes that the fin efficiency in the flooded region is one. If $\eta_f < 1$, one should divide equation (45) by the surface efficiency, η.

5. VALIDATION OF THE PREDICTIVE MODEL

Figure 5 shows the ability of the model to predict the condensation rate on horizontal integral fin tubes. The data bank includes data on 80 tube geometries from 14 different investigators and seven different fluids. Table 1 lists the data sources, the fluids, and the key fin dimensions. The table also shows the ΔT for the predicted point, and the calculated fin efficiency at the point. The fluids include water (high surface tension) and refrigerants (low surface tension). The range of the geometries and fluids tested include:

(1) Fluids: water, methanol, n-pentane, R-11, R-12, R-22 and R-113.

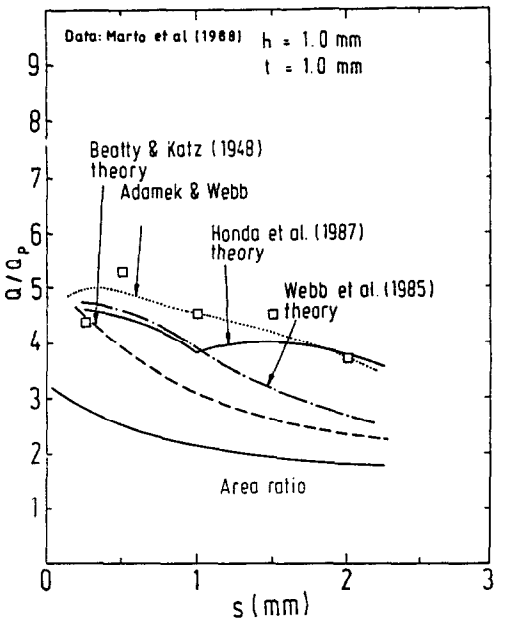

FIG. 6. Evaluation of the ability of various models to predict the R-113 data of Marto *et al.* [19] on 1 mm high × 1 mm thick rectangular fins, for 200–800 fins/m.

(2) Fin spacing at base: 0.06–10 mm.
(3) Fin height: 0.29–3.6 mm.
(4) Fin thickness: 0.06–1.0 mm.

Figure 5 shows the ratio $(Q_{pred} - Q_{exp})/Q_{exp}$ vs fins/m, where subscripts pred and exp are the predicted and experimental values, respectively. The model was adapted to account for the appropriate fin shape (trapezoidal or rectangular) and fin efficiency was included in the calculation. Except for six data points, the data are predicted within ±15%. We feel that this agreement with the data is very good, considering the following uncertainties in the data:

(1) The fin tip radius R_0 was not generally given by the authors. The predictions assumed $R_0 = 0.05t$.

(2) Some of the authors did not precisely describe their fin geometry. Missing dimensions included the fin tip radius, the radius at the fin root, and the spacing at the fin root.

(3) In general, the fin thermal conductivity was not given for the tubes, all of which were copper. We assumed a value of 350 W m^{-2} K^{-1}.

(4) Uncertainty regarding the fluid properties used by the different investigators. Krauss and Stephan [18] have observed that there is a significant difference in the reported property data of the refrigerants. For example, published thermal conductivity data for R-113 at 300 K differs from 0.67 to 0.9 W m^{-2} K^{-1}.

Figures 6 and 7 show the ability of the model to predict the effect of fin spacing for 1.0 mm fin height fins of rectangular cross-section for the R-113 data of Marto *et al.* [19]. Figure 6 is for 1.0 mm fin thickness,

Table 1. Test data predicted (fixed dimensions: $R_0 = 0.05t_t$, $\omega = \pi/4$ rad)

Author(s)	Fluid	D_r	Shape†	h (mm)	t_t (mm)	t_b (mm)	Fins/m	ΔT (°C)	η_r	T_{sat} (°C)	ω' (rad)
Marto *et al.* [19]	R-113	21.0	R	1	1		200, 333, 400, 667, 800	15	0.99	48	0.785
	R-113	21.0	R	1	0.5		400, 500, 667, 1000, 1333	15	0.98	48	0.785
	R-113	21.0	R	1	0.75		364, 444, 571, 800	15	0.99	48	0.785
	R-113	23.0	R	2	1		333, 400, 500	15	0.98	48	0.785
	R-113	21.0	R	0.5	1		333, 400	15	0.99	48	0.785
	R-113	22.0	R	1.5	1		333, 400, 500	15	0.98	48	0.785
Masuda and Rose [20]	R-113	12.7	R	1.6	0.5		400, 500, 667, 1000	10	0.97	48	0.785
Honda and Nozu [23]	R-113	15.8	T	1.46	0.28	0.4	1020	5	0.96	48–67	0.744
	R-113	17.0	T	0.92	0.18	0.3	1551	5	0.97	48–67	0.720
	R-113	16.8	R	1.13	0.1		2000	5	0.92	48–67	0.785
Wanniarachchi *et al.* [21]	Water	19.0	R	1	1		100, 200, 350, 400, 500, 667	30	0.88	100	0.785
	Water	19.0	R	1	1		100, 200, 350, 400, 500, 667	10	0.87	100	0.785
	Water	19.1	R	1	0.5		500	27	0.83	100	0.785
	Water	19.1	T	1	0.017	0.5	500	27	0.81	100	0.548
Yau *et al.* [22]	Water	14.7	R	1.6	0.5		95, 154, 222, 400, 500, 667, 1000	25	0.76	100	0.785
Honda and Nozu [24]	Methanol	15.8	T	1.46	0.28	0.4	1020	5	0.87	65–76	0.744
	Methanol	17.0	T	0.92	0.18	0.3	1551	5	0.90	65–76	0.720
	Methanol	16.8	R	1.13	0.1		2000	5	0.81	65–76	0.785
Katz and Geist [25]	Water	15.8	T	1.52	0.36	0.6	630	42	0.81	43	0.710
Beatty and Katz [9]	n-Pentane	15.8	T	1.46	0.33	0.6	608	33	0.97	43	0.693
	R-22	15.8	T	1.46	0.33	0.6	608	20	0.97	19	0.693
	R-22	19.5	T	3.54	0.34	0.9	270	20	0.95	30	0.710
Henrici [26]	R-12	15.9	T	1.32	0.30		770	5	0.96	35	
	R-12	19.0	T	1.38	0.30		561	5	0.97	35	
	R-12	20.0	T	2	0.50		435	5	0.86	35	
	R-12	20.0	T	3.6	0.36		396	5	0.88	35	
Webb *et al.* [6]	R-11	15.9	T	1.5	0.2	0.45	748, 1020	5	0.96	35	0.702
	R-11	15.9	T	0.89	0.3	0.45	748	5	0.97	35	0.702
	R-11	17.2	T	0.89	0.2	0.29	1378	5	0.96	35	0.735
Sukhatme *et al.* [27]	R-11	23.4	T	0.46	0.09	0.25	1417	5	0.98	35–52	0.613
	R-11	22.6	T	0.71	0.09	0.34	1417	5	0.98	35–52	0.611
	R-11	22.8	T	0.92	0.09	0.41	1417	5	0.98	35–52	0.611
	R-11	22.6	T	1.22	0.09	0.52	1417	5	0.98	35–52	0.611
	R-11	23.4	T	0.46	0.09	0.42	1417	5	0.98	35–52	0.441

† R = rectangular, T = trapezoidal.

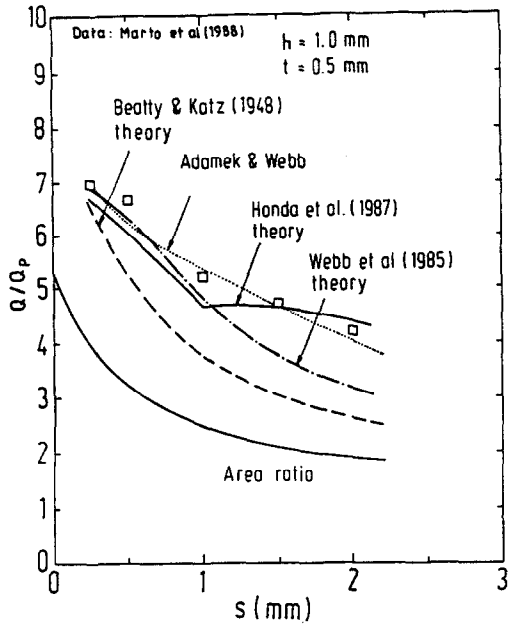

FIG. 7. Evaluation of the ability of various models to predict the R-113 data of Marto *et al.* [19] on 1 mm high × 0.5 mm thick rectangular fins, for 400–1333 fins/m.

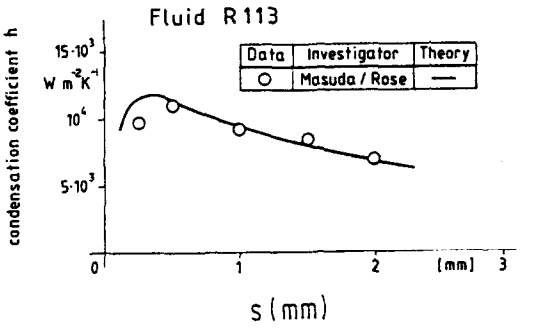

FIG. 8. Evaluation of the ability of the proposed model to predict the R-113 data of Masuda and Rose [20] on 1.6 mm high × 0.6 mm thick rectangular fins, for 600–1000 fins/m.

and Fig. 7 is for 0.5 mm thickness. The ordinate is the enhancement ratio Q/Q_p, where Q_p is for a plain tube of outside diameter D_r. The value of ΔT is the same for the plain and finned tubes. The present model shows excellent ability to predict the data. Also shown in Figs. 6 and 7 are predictions for the models of Honda and Nozu [7], Webb *et al.* [6] and Beatty and Katz [9]. The Beatty and Katz model assumed gravity drainage and no condensate retention. The present model is superior to the other models. The figures also show that the highest performance occurs for fin spacings in the range of 0.5 mm. For the same fin spacing, the 0.5 mm thick fins give higher performance. This occurs for two reasons: (1) the condensate retention angle is larger for the thicker fins, and (2) because the fins/m is less for the greater fin thickness. Figure 6 shows that the increasing condensate retention angle causes a smaller enhancement ratio for the $s = 0.25$ fins than for the $s = 0.5$ mm fins. As the fin spacing decreases, for constant fin thickness, there is a greater possibility for a thick condensate layer to exist at the fin base. Therefore they will be negligible on the root dimension of the tube.

Figure 8 shows that the model does an excellent job of predicting the R-113 data of Masuda and Rose [20]. These fins have a rectangular cross-section.

Figure 9 compares the predicted and experimental Q vs fin spacing for the steam data of Wanniarachchi *et al.* [21] and Yau *et al.* [22]. These data are for rectangular fins having $h = t = 1$ mm. The greatest uncertainty in the prediction occurs for fin spacings at which the interface root radius (R) approaches $s/2$. As the fin spacing is reduced, condensation on the tube root surface becomes negligible, whereas at a higher fin spacing there is a relatively high condensation on the root surface.

The steam data of Wanniarachchi *et al.* [21] are used to validate the ability of the model to predict the effect of fin height for 1.0 mm fin spacing and thickness. The excellent agreement validates the use of equation (32) to predict the drainage in region L_{65} by a gravity drained model. Again, the present model shows better predictive ability than the other models, as shown in Fig. 10.

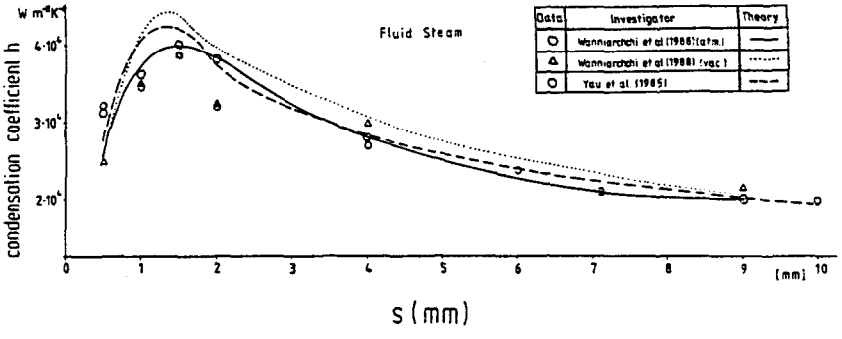

FIG. 9. Evaluation of the ability of the proposed model to predict the steam data of Wanniarachchi *et al.* [21] and Yau *et al.* [22] on 1 mm high × 1 mm thick rectangular fins, for 95–1000 fins/m.

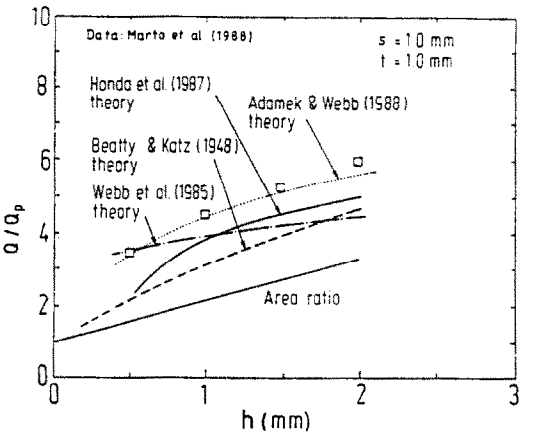

FIG. 10. Evaluation of the ability of various models to predict the R-113 data of Marto *et al.* [19] on 1 mm rectangular fins, for 0.5, 1, 1.5 and 2 mm fin heights.

6. CONCLUSIONS

(1) This paper presents a simple, analytically based model to predict the condensation coefficient on horizontal, integral fin tubes having fins of rectangular or trapezoidal cross-section. The model divides the fin profile into several surface tension or gravity drained regions.

(2) The model was validated by evaluating its ability to predict the data of seven different fluids on 80 different finned tube geometries. The model was shown to predict 74 of the tubes within $\pm 15\%$.

(3) Theoretical relations are also provided to account for the effect of fin efficiency in the calculations.

REFERENCES

1. R. L. Webb, S. T. Keswani and T. M. Rudy, Investigation of surface tension and gravity effects in film condensation, 7th Int. Heat Transfer Conf., Munich, F.R.G. (1982).
2. T. M. Rudy and R. L. Webb, An analytical model to predict condensate retention on horizontal integral-fin tubes, *J. Heat Transfer* **107**, 361–368 (1985).
3. R. Gregorig, Film condensation on finely rippled surfaces with consideration of surface tension, *Z. Angew. Math. Phys.* **5**, 36–49 (1954).
4. T. Adamek, Bestimmung der Kondensationgrössen auf feingewellten Oberflächen zur Auslegung optimaler Wandprofile, *Wärme- und Stoffübertr.* **15**, 255–270 (1981).
5. H. Honda, A prediction method for heat transfer during film condensation on horizontal low integral fin tubes, *ASME HTD* **38**, 107–114 (1984).
6. R. L. Webb, T. M. Rudy and M. A. Kedzierski, Prediction of the condensation coefficient on horizontal integral-fin tubes, *J. Heat Transfer* **107**, 369–376 (1985).
7. H. Honda and S. Nozu, A prediction method for heat transfer during film condensation on horizontal low integral-fin tubes, *J. Heat Transfer* **108**, 218–225 (1986).
8. R. L. Webb, Enhancement of film condensation, *Int. Commun. Heat Mass Transfer* **15**, 475–508 (1988).
9. K. O. Beatty and D. L. Katz, Condensation of vapors on outside of finned tubes, *Chem. Engng Prog.* **44**, 55–70 (1948).
10. T. M. Rudy and R. L. Webb, Theoretical model for condensation on horizontal integral-fin tubes, *Heat Transfer A.I.Ch.E. 79*, No. 225. A.I.Ch.E., New York (1983).
11. W. Nusselt, Die Oberflächenkondensation des Wasserdampfes, *Z. Ver. Deut. Ing.* **60**, 541–569 (1916).
12. V. G. Rifert, Teplomassoobmen-V Materialy V (pjatoj) veseojuznojkonferencii po teplomassobmenju, Minsk (1976).
13. T. M. Rudy, A theoretical and experimental study of condensation on single, integral-fin tubes, Ph.D. Thesis, The Pennsylvania State University (1982).
14. D. G. Thomas, Enhancement of film condensation rate on vertical tubes by longitudinal wires, *A.I.Ch.E. Jl* **14**, 644–649 (1968).
15. H. Honda, S. Nozu and B. Uchima, A generalized prediction method for heat transfer during film condensation on a horizontal low finned tube, *ASME–JSME Thermal Engng Joint Conf.*, Vol. 4, pp. 385–392 (1987).
16. T. Adamek and R. L. Webb, Prediction of film condensation on vertical finned plates and tubes: a model for the drainage channel, *Int. J. Heat Mass Transfer* **33**, 1737–1749 (1990).
17. T. Adamek, Rechenmodell der Filmkondensation an engberippten Kondensatorrohren, *Wärme- und Stoffübertr.* **19**, 145–147 (1985).
18. R. Krauss and K. Stephan, Thermal conductivity of refrigerants in a wide range of temperature and pressure, *J. Phys. Chem. Ref. Data* **18**(1), 43–76 (1989).
19. P. J. Marto, D. Zebrowski, A. S. Wanniarachchi and J. W. Rose, Film condensation of R-113 on horizontal finned tubes. In *Proc. 1988 National Heat Transfer Conf.* (Edited by H. R. Jacobs), HTD-96, Vol. 2, pp. 583–592. ASME (1988).
20. H. Masuda and J. W. Rose, An experimental study of condensation of refrigerant R113 on low integral-fin tubes. In *Heat Transfer Science and Technology* (Edited by B.-X. Wang), pp. 480–487. Hemisphere, Washington, DC (1987).
21. A. Wanniarachchi, P. Marto and J. Rose, Filmwise condensation of steam on horizontal tubes with rectangular-shaped fins, *ASME Symp.* **HTD47**, 93–99 (1986).
22. K. K. Yau, J. R. Cooper and J. W. Rose, Effect of fin spacing on the performance of horizontal integral-fin condenser tubes, *J. Heat Transfer* **107**, 377–383 (1985).
23. H. Honda and S. Nozu, Augmentation of condensation on horizontal finned tubes by attaching a porous drainage plate, *Proc. ASME–JSME Thermal Engng Joint Conf.*, Vol. 3, pp. 289–295 (1983).
24. H. S. Honda and S. Nozu, Effect of drainage strips on the condensation heat transfer performance of horizontal finned tubes. In *Heat Transfer Science and Technology* (Edited by B.-X. Wang), pp. 455–462. Hemisphere, Washington, DC (1987).
25. D. L. Katz and J. M. Geist, Condensation of six finned tubes in a vertical row, *Trans. ASME* **70**, 907–914 (1948).
26. K. Henrici, Kondensation von Frigen 12 und Frigen 22 an glatten und berippten Rohren, Dissertation, TU Karlsruhe (1961).
27. S. P. Sukhatme, B. S. Fagadish and P. Brabhakaran, Heat transfer during film condensation on enhanced surface horizontal condenser tubes. Presented at 9th Heat Mass Transfer Conf., Fudiau Fud of Science, Baugalon, India (1987).

APPENDIX A. FIN EFFICIENCY FOR RECTANGULAR OR TRAPEZOIDAL FINS

Analytical expressions for the temperature distribution in rectangular fins are developed. The results can be applied to trapezoidal fins by using the average fin thickness. Separate

fin efficiency expressions are required for the flooded and the unflooded regions.

The following assumptions were used to define the problem and simplify the solution:

(1) Steady state heat transfer.
(2) One-dimensional heat conduction in the fin.
(3) The vapor surrounding the fin is saturated and of uniform temperature.

Unflooded region

Fin efficiency calculations usually assume the heat transfer coefficient is constant over the fin length. We do not use this assumption. Surface tension drained condensation typically has large heat transfer coefficients at the fin tip, and small heat transfer coefficients at the fin root. The assumption of a constant heat transfer coefficient will overpredict the heat transfer to the fin. Our analysis calculates the local condensation coefficient as $k/\delta(x)$, where $\delta(x)$ is the local condensate film thickness.

An energy balance on a differential element of the rectangular fin yields

$$k_w \frac{t}{2}\left(\left.\frac{d\theta}{dx}\right|_{x+dx} - \left.\frac{d\theta}{dx}\right|_{x}\right) = \frac{k}{\delta_{01}}\theta\, dx \tag{A1}$$

where k_w is the thermal conductivity of the fin, t is the fin thickness, and $\theta = T_{sat} - T_w$. Equation (A1) states that the heat of condensation rate entering the differential element is equal to the difference between the heat conducted into and out of the incremental volume.

Equation (A1) is first soived for region L_{01}, with x measured from point 0. Solving equation (A1) for the temperature gradient in the fin at location x gives

$$\frac{d\theta}{dx} = \frac{2k}{tk_w}\int_0^x \frac{\theta}{\delta_{01}(x)}\, dx. \tag{A2}$$

The film thickness $\delta_{01}(x)$ in region L_{01} is given by equation (15a) in the text. Recognizing that both x and $\Delta T \equiv \theta$ are functions of x, we write equation (15a) as

$$\delta_{01}(x) = \left(\frac{1}{f_{01}}\frac{4k\eta}{\lambda\rho}\int_0^x \theta(x)\, dx\right)^{1/4}. \tag{A3}$$

Substitution of equation (A3) for $\delta(x)$ in equation (A2) gives

$$\left.\frac{d\theta}{dx}\right|_x = \frac{2k}{k_w t}\left(\frac{f_{01}\lambda\rho}{4k\eta}\int_0^x \frac{\theta(\xi)}{\left(\int_0^\xi \theta(\tau)\, d\tau\right)^{1/4}} d\xi\right)^{1/4}. \tag{A4}$$

Let the grouping of constants in equation (A4) be defined as

$$c_0 = \frac{2k}{k_w t}\left(\frac{f_{01}\lambda\rho}{4k\eta}\right)^{1/4}. \tag{A5}$$

Evaluation of the integral on the right side of equation (A4) gives

$$\int_0^x \frac{\theta(\xi)}{\left(\int_0^\xi \theta(\tau)\, d\tau\right)^{1/4}} d\xi = \frac{4}{3}\left[\int_0^x \theta(\xi)\, d\xi\right]^{3/4}. \tag{A6}$$

Substitution of equation (A6) in equation (A4) gives the following differential equation

$$\theta''(x) = c_1\left(\frac{1}{\theta'(x)}\right)^{1/3}\theta(x) \tag{A7}$$

where

$$c_1 = \frac{3}{4}\left(\frac{4c_0}{3}\right)^{4/3}. \tag{A8}$$

Substituting $p[x(\theta)] \equiv \theta'(x)$ in equation (A7) and integrating from $x = 0$ yields

$$p(\theta) = \frac{d\theta}{dx} = (p_0^{7/3} + \tfrac{7}{8}c_1(\theta^2 - \theta_0^2))^{3/7} \tag{A9}$$

where p_0 and θ_0 denote the initial conditions at the fin tip ($x = 0$)

$$p_0 = \left.\frac{d\theta}{dx}\right|_{x=0} = \frac{2(\dot{m}_{01'} + \dot{m}_{1'2'})}{\lambda k_w t} \tag{A10}$$

and

$$\theta_0 = \Delta T(x = 0). \tag{A11}$$

The relation between the temperature difference $\theta \equiv T_{sat} - T_w$ and the x-coordinate is obtained by substituting equation (A9) in equation (A12) and performing the integration

$$x(\theta) = \int_{\theta_0}^{\theta} \frac{1}{p(\theta)}\, d\theta. \tag{A12}$$

When the heat flow in the fin crosses from region L_{01} into region L_{12}, we start the analysis again, replacing the f_{01} and δ_{01} by f_{12} and δ_{12}. The film thickness formula for δ_{12} also contains an additional constant, which accounts for the film thickness at point $x = l_{01}$. However, this constant is cancelled by the differentiation process, hence the analysis for L_{02} is analogous to that for L_{01}.

Similarly, when the heat flow within the fin crosses the L_{12}–L_{23} boundary, we replace f_{12} and δ_{12} by f_{23} and δ_{23}. If we denote the heat flow in the fin at point 3 ($x = l_{01} + l_{12} + l_{23}$) by q_{act} (actual q) and compare to q_{max} (maximum q for zero temperature gradient in the fin), we obtain the fin efficiency, which is defined as

$$\eta_f = q_{act}/q_{max}. \tag{A13}$$

The q_{max} is given by

$$q_{max} = (\dot{m}_{1'2'} + \dot{m}_{01'} + \dot{m}_{01} + \dot{m}_{12} + \dot{m}_{23})/\lambda \tag{A14}$$

where the $\dot{m}_{ik}$ are computed assuming the local fin temperature is equal to that at the fin base.

Flooded region

In the flooded fraction of the tube, condensation occurs on the fin tip. Because the fins are quite short, a one-dimensional conduction model is acceptable. Assuming no heat transfer from the sides of the fin in the flooded region, we may write the equation for heat conduction in a fin of constant thickness, t

$$q = k_w A_b (T_{w,t} - T_{w,r})/h \tag{A15}$$

where $T_{w,r}$ is the fin base temperature, $T_{w,t}$ is the fin tip temperature, and h is the fin height. The heat transferred by convection from the fin tip is

$$q = h_t A_t (T_{sat} - T_{w,t}). \tag{A16}$$

Combining equations (A15) and (A16) and solving for $T_{w,t}$ gives for a rectangular fin ($A_t = A_b$)

$$T_{w,t} = (T_{w,r} + Nu_t T_{sat})/(Nu_t + 1) \tag{A17}$$

where $Nu_t = h_t h/k_w$. Substitution of equation (A17) in equation (A16) gives

$$q = h_t A_t (T_{sat} - T_{w,r})/(Nu_t + 1). \tag{A18}$$

Let q_{max} be the heat transfer rate for a fin, having $T_{w,t} = T_{w,r}$, which is given by

$$q_{max} = h_{t,\infty} A_t (T_{sat} - T_{w,r}) \tag{A19}$$

where $h_{t,\infty}$ is the condensation coefficient if $T_{w,t} = T_{w,r}$. The fin efficiency is defined as q/q_{max}, and is the ratio of equations (A18) and (A19), giving

$$\eta_f = h_t/[h_{t,\infty}(Nu_t + 1)]. \tag{A20}$$

Using $\dot{m}_t\lambda = h_t A_t(T_{sat}-T_{w,t})$ and $\theta \equiv (T_{sat}-T_w)$, equation (A20) may be written as

$$\eta_f = \dot{m}_t\theta_{t,x}/[\dot{m}_{t,\infty}\theta_t(Nu_t+1)] \quad \text{(A21)}$$

where the terms $\dot{m}_{t,\infty}$ and $h_{t,x}$ are for a fin of infinite thermal conductivity. The fin tip efficiency may be iteratively determined by assuming a fin tip temperature and using equations (A15), (A16) and (A21) to check for convergence of the fin tip temperature.

APPENDIX B. CONDENSATION MODES ASSOCIATED WITH THE CONDENSATE LEVEL Δ

Adamek and Webb [16] describe the different modes of condensation that exist in the channel of a vertical finned plate. These same modes are applicable to the present finned tube geometry. The appropriate modes are summarized here.

The magnitude $R(z)$ varies between R_{min} at the top of the tube ($z = 0$) and its maximum value R_{max} at $\Psi = \Psi_0$ ($z = z_u$), which is limited to $R \leqslant s/2$. Hence, for small fin heights h and small fin spacings s, some of the condensation areas may vanish. As long as $R(z) \leqslant s/2$, the condensate level Δ remains zero and the fin height h (Fig. 3(a)) is equal to the sum of the components

$$h = R^*(z)+l_{01}(z)+l_{12}(z)+l_{23}(z). \quad \text{(B1)}$$

When the $R(z)$ joins at the center of the channel, the condensate level $\Delta(z)$ starts to increase. Then h is expressed by

$$h = R^*(z)+l_{01}(z)+l_{12}(z)+l_{23}(z)+\Delta(z). \quad \text{(B2)}$$

When $\Delta(z) > 0$, the condensation rate at the fin base is assumed to be zero. For this case

$$R^* = s/2. \quad \text{(B3)}$$

Three possible condensation modes may exist on the fin side. They are modes A, B, and C as described below.

Mode A: $h-[R^*(z)+l_{01}(z)+l_{23}(z)+\Delta(z)] \geqslant 0.$ (B4)

The difference of the terms on the left-hand side yields the length $l_{12}(z)$. Mode A occurs for the increments near the top of the tube and yields the highest performance. If equation (B4) is true, equations (23)–(27) are used to calculate l_{12} and l_{23}, respectively.

Mode B: $h-[R^*(z)+l_{23}(z)+l_{01}(z)+\Delta z] \leqslant 0.$ (B5)

Mode B is initiated following Mode A and is distinguished by the condition $l_{12}(z) = 0$. Then, $l_{23}(z)$ is given by

$$l_{23}(z) = h-[R^*(z)+l_{01}(z)+\Delta(z)] \quad \text{(B6)}$$

rather than by equation (27).

Mode C: $h-[R^*(z)+l_{01}(z)+\Delta(z)] \leqslant 0.$ (B7)

This mode exists when the condensate thickness (Δ) is so thick that both $l_{12}(z)$ and $l_{23}(z)$ vanish. Condensation occurs only at the fin tip area. Moreover, the circular interface of the drainage region may cover the thin film area L_{01} at the fin tip.

Modes D, E and F describe conditions that affect condensation at the fin base.

Mode D: $s/2-[R^*(z)+l_{54}(z)] \geqslant 0.$ (B8)

The length $l_{65}(z)$ is given by the difference of the two terms on the left-hand side of equation (B8). When $R(z)$ increases, $l_{65}(z)$ decreases. When $l_{65}(z)$ becomes zero, we attain the Mode E.

Mode E: $s/2-[R^*(z)+l_{54}(z)] \leqslant 0$ (B9)

but $l_{54}(z)$ is not calculated by equation (27). If Mode E exists, one should calculate length $l_{54}(z)$ by

$$l_{54}(z) = s/2-R^*(z). \quad \text{(B10)}$$

When $l_{54}(z) = 0$, $R^*(z) = s/2$ and the condensate level $\Delta(z)$ begins to rise. Then the condensation at the fin base is negligible. This situation is called mode F.

PREDICTION DE LA CONDENSATION EN FILM SUR DES TUBES HORIZONTAUX A AILETTES INTEGRALES

Résumé—On présente un modèle analytique pour la prédiction de la condensation en film sur des tubes horizontaux à ailettes intégrales. Ce modèle tient compte de la condensation sur toutes les surfaces dans les régions noyées ou non, et il inclut l'effet de l'efficacité de l'ailette. Il est basé sur des principes simples et il permet des calculs à la main ou par ordinateur. Il est applicable à des ailettes avec deux profils différents: le profil continu spécial décrit par Gregorig, Adamek, Webb ou la section droite rectangulaire ou trapézoïdale. Le modèle est validé par sa capacité à prédire un large domaine de données expérimentales. Ces données qui incluent l'eau, le méthanol, le n-pentane, R-11, R-12, R-22 et R-113 sont prédites pour 80 géométries différentes de tube dans l'intervalle ±15%. Les prédictions de ce modèle sont comparées à celles données par d'autres modèles proposés par Webb *et al.*, Honda et Nozu, et Beatty et Katz.

BERECHNUNG DER FILMKONDENSATION AUF WAAGERECHTEN INTEGRAL-RIPPENROHREN

Zusammenfassung—In dieser Arbeit wird ein analytisches Modell zur Berechnung der Filmkondensation an waagerechten Integral-Rippenrohren vorgestellt. Das Modell berücksichtigt Kondensation an allen Oberflächen in den überfluteten und nicht überfluteten Bereichen, der Einfluß des Rippenwirkungsgrades ist ebenfalls enthalten. Das Rechenverfahren ist auf recht einfachen Grundprinzipien aufgebaut und kann leicht für Berechnungen von Hand oder mit dem Computer angewandt werden. Das Rechenmodell ist für Rippen mit zwei unterschiedlichen Grundformen des Profils geeignet: einmal die speziellen kontinuierlichen Profile, die bereits früher von Gregorig, Adamek und Webb beschrieben worden sind, zum anderen Rippen mit rechteckigem oder trapezförmigem Querschnitt. Das Modell wird mit Hilfe von experimentellen Daten in weiten Bereichen bestätigt. Diese Daten wurden mit Wasser, Methanol, n-Pentan, R-11, R-12, R-22 und R-113 ermittelt. Dabei wurden 80 unterschiedliche Rohrgeometrien verwendet, die Übereinstimmung liegt innerhalb ±15%. Abschließend werden die Ergebnisse des vorgestellten Modells mit früheren Modellrechnungen verglichen, nämlich denen von Webb *et al.*, Honda und Nozu sowie Beatty und Katz.

ОПРЕДЕЛЕНИЕ ПЛЕНОЧНОЙ КОНДЕНСАЦИИ НА СБОРКЕ ГОРИЗОНТАЛЬНЫХ ОРЕБРЕННЫХ ТРУБ

Аннотация—Предложена аналитическая модель для определения пленочной конденсации на сборке горизонтальных оребренных труб. Модель учитывает конденсацию на всех поверхностях в затопленных и незатопленных областях, а также эффективность оребрения. В то же время она основана на довольно простых принципах и применима для расчетов с использованием и без использования ЭВМ. Модель применяется для ребер с двумя различными основными профилями: особой сплошной формы, ранее описанной Грегоригом, Адамеком и Веббом, или для ребер с прямоугольным или трапецеидальным поперечными сечениями. Адекватность модели подтверждается ее применимостью для расчета большого количества экспериментальных данных для воды, н-пентана, R-11, R-12, R-22 и R-113. Эти результаты получены для 80 различных геометрий трубы с точностью до $\pm 15\%$. Сравниваются расчеты по данной модели и по моделям, ранее предложенным Руди и др., Хонда и Нозу, а также Битти и Кацом.